

# Extreme phase sensitivity in systems with fractal isochrons

A. Mauroy\*

*Department of Electrical Engineering and Computer Science,  
University of Liège, 4000 Liège, Belgium*

I. Mezić†

*Department of Mechanical Engineering,  
University of California Santa Barbara, Santa Barbara, CA 93106, USA*

## Abstract

Sensitivity to initial conditions is usually associated with chaotic dynamics and strange attractors. However, even systems with (quasi)periodic dynamics can exhibit it. Here we report on the fractal properties of the isochrons of some continuous-time asymptotically periodic systems. We define a measure of phase sensitivity that we call *the phase sensitivity coefficient* and show that it is directly related to the capacity dimension of the isochrons. Similar results are also obtained with discrete-time systems. We apply the framework to popular models of bursting neurons, showing that elliptic bursting neurons—characterized by isochrons of high fractal dimensions—exhibit a very sensitive phase response and are therefore unreliable.

Keywords: isochrons, fractals, transient chaos, bursting neurons

---

\*Electronic address: a.mauroy@ulg.ac.be

†Electronic address: mezić@enr.ucsb.edu

## I. INTRODUCTION

Isochrons and asymptotic phase play a central role for the study of asymptotically periodic systems. The isochrons have been introduced in [29] as the sets of initial states that converge to the same trajectory on the limit cycle. Equivalently, they are the sets of states that share the same *asymptotic phase* [28]. The notions of isochrons and asymptotic phase are of paramount importance to capture the system sensitivity to external perturbations [23, 25]. Indeed, an external perturbation has a significant long-term effect on the system only if the perturbed and unperturbed trajectories lie on different isochrons (associated with an important asymptotic phase difference). Beyond their applications to sensitivity analysis, isochrons and asymptotic phase also lead to a powerful phase reduction of the dynamics that is widely used for studying synchronization properties of coupled limit-cycle systems (see e.g. [1, 2, 9, 13]).

Thanks to a numerical method based on the Koopman operator framework and introduced in [17], it has been observed recently that isochrons may exhibit a fractal geometry [18]. (Note that a similar phenomenon was also discussed in [20] for the asymptotic phase of a discrete-time map.) As shown in the present paper, fractal isochrons result from the existence of a fractal phaseless set in a region of high finite-time Lyapunov exponents, and are naturally explained by a transient chaotic regime [31] in presence of a stable limit cycle. The empirical observation of fractal isochrons is related to an extremely high phase sensitivity of the system, a property which is not associated with chaotic dynamics and with the existence of a strange attractor.

In this paper, we propose a theoretical framework to quantify the fractal properties of isochrons and their effect on sensitivity. To that end, we define *the phase sensitivity coefficient* that quantifies the overall phase sensitivity of the system. Using a result of [19], we prove that this coefficient is closely related to the capacity dimension [3] of the isochrons. This implies that when the isochrons are fractal, a significant decrease of the intensity of a noise perturbation can only slightly reduce the average uncertainty on the phase. In addition, the framework is applied to different types of bursting neurons, showing in particular that elliptic bursting neurons are highly sensitive (i.e. with fractal isochrons of high dimension) and therefore characterized by unreliable responses to external inputs. Their (finite) phase response curve is also shown to be fractal.

The paper is organized as follows. In Section II, we rigorously define the notions of asymptotic phase and isochrons. Section III presents basic observations and descriptions of the fractal properties of the isochrons. The relationship between phase sensitivity and fractal dimension of the isochrons is discussed in Section IV. We apply the results to bursting neuron models in Section V. Finally, concluding remarks are given in Section VI.

## II. ASYMPTOTIC PHASE AND ISOCHRONS

We consider a nonlinear system  $\dot{\mathbf{x}} = \mathbf{F}(\mathbf{x})$ , with  $\mathbf{x} \in \mathbb{R}^N$  and  $\mathbf{F}$  analytic, which generates a flow  $\varphi : \mathbb{R}^+ \times \mathbb{R}^N \rightarrow \mathbb{R}^N$  and admits a periodic orbit  $\Gamma$  of period  $T_0 = 2\pi/\omega_0$ , i.e.  $\varphi(T_0, \mathbf{x}^\gamma) = \mathbf{x}^\gamma$  with  $\mathbf{x}^\gamma \in \Gamma$ . Each point  $\mathbf{x}^\gamma$  of the periodic orbit is associated with a phase  $\theta \in \mathbb{S}^1$  according to the mapping  $\mathbf{x}^\gamma(\theta) = \varphi((\theta/2\pi)T_0, \mathbf{x}_0^\gamma)$ , where  $\mathbf{x}_0^\gamma = \mathbf{x}^\gamma(0)$  is an arbitrarily chosen point of  $\Gamma$  [28].

If  $\Gamma$  is an asymptotically stable limit cycle with a basin of attraction  $\mathcal{B} \subseteq \mathbb{R}^N$ , the (asymptotic) phase function  $\Theta : \mathcal{B} \rightarrow \mathbb{S}^1$  assigns the same phase  $\theta$  to the initial states converging to the same trajectory on the limit cycle, i.e.

$$\Theta(\mathbf{x}) = \theta \quad \Leftrightarrow \quad \lim_{t \rightarrow \infty} \|\varphi(t, \mathbf{x}) - \varphi(t, \mathbf{x}^\gamma(\theta))\| = 0. \quad (1)$$

The level sets of  $\Theta$ —i.e. the sets of states that share the same asymptotic behavior—are the so-called isochrons [29]

$$\mathcal{I}_\theta = \{\mathbf{x} \in \mathcal{B} | \Theta(\mathbf{x}) = \theta\}.$$

If the limit cycle is normally hyperbolic, the isochrons  $\mathcal{I}_\theta$  are co-dimension-1 manifolds that invariantly foliate the basin of attraction [8].

Figure 1 shows the asymptotic phase and 5 isochrons for the Van der Pol model. We note that the phase function is not defined at the unstable fixed point at the origin. This is the *phaseless set*  $\mathcal{S}$ , which corresponds more generally to the boundary of the basin of attraction  $\mathcal{B}$ . It was shown in [6] that the values of the phase function evaluated on any neighborhood of the phaseless set span the entire circle  $\mathbb{S}^1$ . In other words, the isochrons come arbitrarily close to the phaseless set.

*a. Numerical computation.* There exist several methods for computing the isochrons of limit cycles (see e.g. [7, 10, 12, 14, 21, 24]). For our purpose, we will use the forward-integration method proposed recently in [17], which is based on the fact that the phase

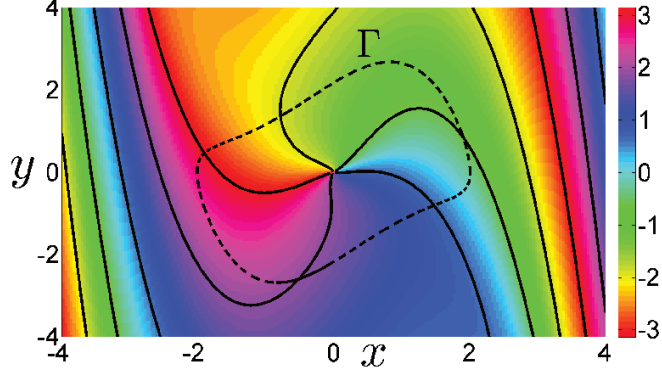


Figure 1: Asymptotic phase and 5 isochrons (equally spaced in phase) for the Van der Pol model  $\dot{x} = y$ ,  $\dot{y} = (1 - x^2)y - x$ . The unstable fixed point at the origin is the phaseless set  $\mathcal{S}$ .

function is related to an eigenfunction of the so-called Koopman operator [20]. (Note that the method presented in [7, 10] precisely solves a partial differential equation which is closely related to the eigenvalue equation for the Koopman operator.) The method is appropriate to deal with the complex geometry of the isochrons that we investigate in this paper. It is also well-suited to the computation of isochrons in non-planar models. Through this framework, the phase function is directly given by the argument  $\angle$  of the Fourier average evaluated along the trajectories, i.e.

$$\Theta(\mathbf{x}) = \angle \left( \lim_{T \rightarrow \infty} \frac{1}{T} \int_0^T g \circ \varphi(t, \mathbf{x}) e^{-i\omega_0 t} dt \right), \quad (2)$$

where  $g \in C^1 : \mathcal{B} \rightarrow \mathbb{C}$  is an arbitrary function (observable) such that the first Fourier coefficient (first harmonic) of the periodic function  $g \circ \varphi(t, \mathbf{x}^\gamma)$  (with  $\mathbf{x}^\gamma \in \Gamma$ ) is nonzero. Note that the state  $\mathbf{x}_0^\gamma \in \Gamma$  associated with the phase  $\theta = 0$  is determined by the specific choice of  $g$ .

The Fourier averages (2) can be easily computed through the numerical integration of trajectories, with the initial conditions on a uniform grid that spans a region of interest in the state space. The isochrons are obtained by plotting the level sets of these Fourier averages.

*b. Discrete time.* The phase function  $\Theta$  can also be defined in the case of discrete-time systems. Consider the map  $\mathbf{x}(t+1) = \mathbf{F}(\mathbf{x}(t))$ ,  $\mathbf{x} \in \mathbb{R}^N$ ,  $t \in \mathbb{N}$ , which generates the flow  $\varphi : \mathbb{N} \times \mathbb{R}^N \rightarrow \mathbb{R}^N$ . We assume that the system admits an invariant set  $\Gamma$ , a topological circle, on which the dynamics has an irrational rotation number  $\nu_0$ . This

invariant set can be characterized as a closure of a dense orbit, i.e.  $\Gamma = \overline{\cup_{t \in \mathbb{N}} \varphi(t, \mathbf{x}^\gamma)}$  for some  $\mathbf{x}^\gamma \in \mathbb{R}^N$ . In this case, there exists a sequence  $\{t_k\}_{1 \leq k \leq \infty}$  such that  $\lim_{k \rightarrow \infty} t_k \nu_0 \bmod 1 = 0$  and  $\lim_{k \rightarrow \infty} \varphi(t_k, \mathbf{x}^\gamma) = \mathbf{x}^\gamma$  for all  $\mathbf{x}^\gamma \in \Gamma$ . To prove this, we have by definition

$$\nu_0 = \lim_{t \rightarrow \infty} \frac{F^t(s(\mathbf{x}^\gamma)) - s(\mathbf{x}^\gamma)}{t},$$

where  $s : \Gamma \rightarrow [0, 1]$  defines a coordinate on the circle  $\mathbb{S}^1([0, 1])$  and  $F$  is the lifting of the map on the circle to real line. Let the sequence  $\epsilon_k$  converge to 0 and define

$$\nu_k = \frac{F^{t_k}(s(\mathbf{x}^\gamma)) - s(\mathbf{x}^\gamma)}{t_k}, \quad (3)$$

where  $F^{t_k}(s(\mathbf{x}^\gamma)) - s(\mathbf{x}^\gamma) \bmod 1 < \epsilon_k$  or  $F^{t_k}(s(\mathbf{x}^\gamma)) - s(\mathbf{x}^\gamma) \bmod 1 > 1 - \epsilon_k$  (we know such  $t_k$  exist due to the fact that every trajectory in the circle is dense). Therefore, it follows from (3) that  $(\nu_k t_k) \bmod 1 < \epsilon_k$  or  $(\nu_k t_k) \bmod 1 > 1 - \epsilon_k$  and thus  $\lim_{k \rightarrow \infty} (\nu_0 t_k) \bmod 1 = 0$ .

Each point  $\mathbf{x}^\gamma$  is associated with a phase  $\theta \in \mathbb{S}^1([0, 2\pi])$  according to the mapping  $\mathbf{x}^\gamma(\theta) = \lim_{k \rightarrow \infty} \varphi(t_k, \mathbf{x}_0^\gamma)$ , where the sequence  $\{t_k\}_{1 \leq k \leq \infty}$  satisfies  $\lim_{k \rightarrow \infty} t_k \omega_0 \bmod 2\pi = \theta$ , with  $\omega_0 = 2\pi \nu_0$ . If the periodic orbit is asymptotically stable with a basin of attraction  $\mathcal{B}$ , the phase function is defined on  $\mathcal{B}$  by (1) and can be computed through the Fourier averages (2) (with a sum replacing the integral). The isochrons can still be defined as the level sets of the phase function, but they are not connected manifolds.

### III. FRACTAL PROPERTIES OF THE PHASE FUNCTION

We consider particular (continuous-time and discrete-time) dynamical systems and show that their associated phase function exhibits fractal patterns, suggesting that the isochrons are fractal. These systems are characterized by a very high phase sensitivity.

#### A. Continuous-time model

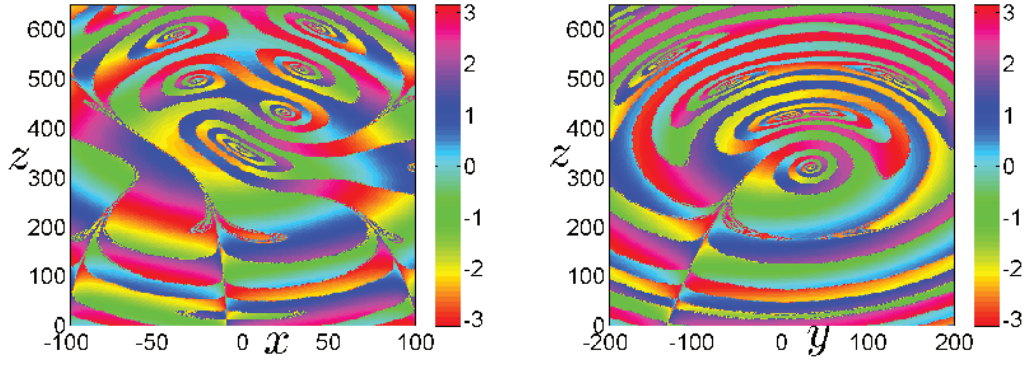
The Lorenz system

$$\begin{aligned} \dot{x} &= \sigma(y - x) \\ \dot{y} &= x(r - z) - y \\ \dot{z} &= xy - bz \end{aligned} \quad (4)$$

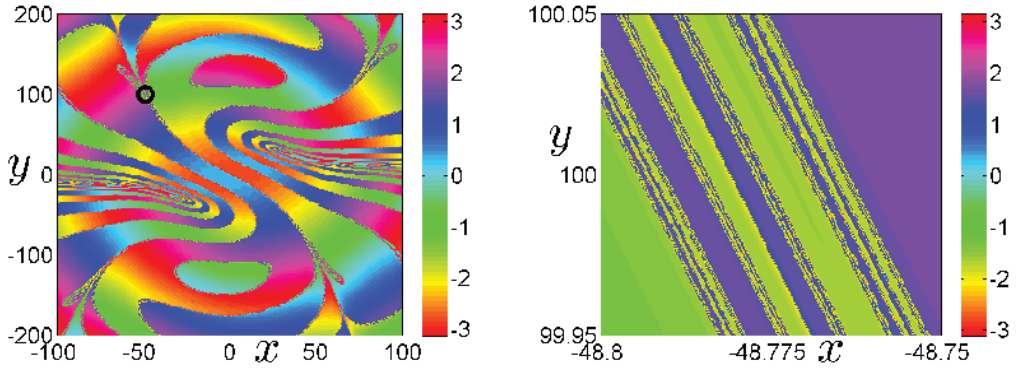
admits a stable limit cycle for the parameters  $\sigma = 10$ ,  $b = 8/3$ , and  $r = 320$ . For this model, Figure 2(a)-(c) shows that the phase function exhibits unusually complex patterns, whose geometry is constrained by the phaseless set (seen on the figures as the region of sharp phase variation). While it is well-known that the phase function and the isochrons may be complicated near the phaseless set (e.g. near an unstable fixed point, see [14, 21]), the remarkable fact relies here in their fractal properties, which is induced by the fractal geometry of the phaseless set itself (see the close-up in Figure 2(d)). Note that, for the sake of clarity, we show only the phase function in Figure 2, the fractal isochrons being mainly concentrated near the phaseless set  $\mathcal{S}$ .

Though never reported before, the fractal property of the phaseless set is a natural consequence of the chaotic transient regime of the system [31]. In presence of chaotic transient, the system admits a chaotic saddle (see e.g. [26])—also called fractal repeller in [5]—which is a fractal invariant set containing the union of all unstable periodic orbits. In other words, trajectories on the chaotic saddle or on the stable manifold of the chaotic saddle do not converge toward the attractor (and trajectories starting very close to this set are typically characterized by a long escape time before converging to the attractor). For asymptotically periodic systems exhibiting chaotic transient, the fractal chaotic saddle and its stable manifold correspond precisely to the phaseless set  $\mathcal{S}$ . Also, for the Lorenz system (4), the phaseless set includes the stable manifold of the saddle node at the origin, which was shown in [19] to have a fractal Cantor-like geometry.

In presence of chaotic transient, the neighborhood of  $\mathcal{S}$  is characterized by a (extremely) high phase sensitivity. Figure 3 shows that two trajectories starting from this region, with very close initial conditions, can have different long-term behaviors reflected in their asymptotic phase. During a time of the order of several limit cycle periods, the two trajectories remain close to the fractal phaseless set  $\mathcal{S}$ , then “escape”  $\mathcal{S}$  and diverge near the  $z$  axis, subsequently reaching different regions of the limit cycle. Note that it is not sensitivity to initial conditions in classical sense, where exponential convergence is forever, but it is the popular notion of sensitivity where small changes in initial conditions can separate the trajectories. As shown in Figure 4, this phenomenon can be captured through the computation of the largest finite-time (or local) Lyapunov exponent [16, 30]. Regions of high finite-time Lyapunov exponent (black regions) are associated with a high sensitivity to initial conditions. By comparing with Figure 2(c), we verify that these regions lie close to the fractal



(a) Phase function in the cross-section  $y = 50$  (b) Phase function in the cross-section  $x = 25$



(c) Phase function in the cross-section  $z = 319$  (d) Close-up in the cross-section  $z = 319$

$z = 319$

Figure 2: (a)-(c) For the Lorenz model (4), the phase function exhibits complex patterns with boundaries characterized by high phase variation (phaseless set). (The cross-section (c) was chosen so that it contains the two unstable fixed points at  $(x, y) \approx \pm(29.17, 29.17)$ .) (d) The phaseless set  $\mathcal{S}$  has a fractal geometry. (The close-up focuses on a region of the cross-section  $z = 319$ , marked with the black circle in (c).)

phaseless set.

## B. Discrete-time model

We consider the following map (taken from [20]):

$$\begin{aligned} x(t+1) &= (1 - \gamma)x(t) + a \sin^2(2\pi y(t)) \\ y(t+1) &= x(t) + y(t) + a \sin(2\pi y(t)) \bmod 1 \end{aligned} \tag{5}$$

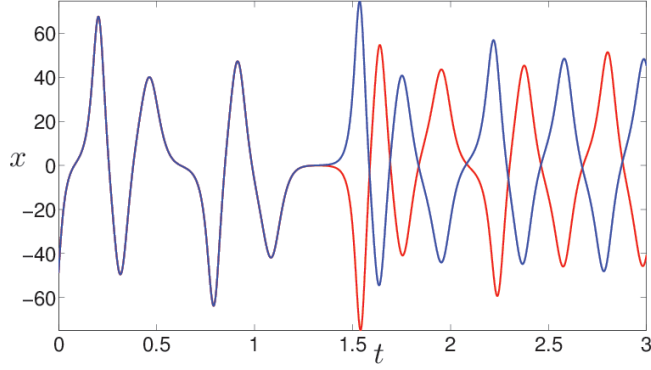


Figure 3: As an illustration of the high phase sensitivity observed near the phaseless set, in the Lorenz system (4), two trajectories with close initial conditions diverge (after a long time period) and exhibit two different asymptotic behaviors on the limit cycle. The initial conditions are chosen in the close-up of Figure 2(d) ( $x(0) = -48.7810$  (red trajectory) and  $-48.7810 - 2 \times 10^{-4}$  (blue trajectory),  $y(0) = 100$ ,  $z(0) = 319$ ).

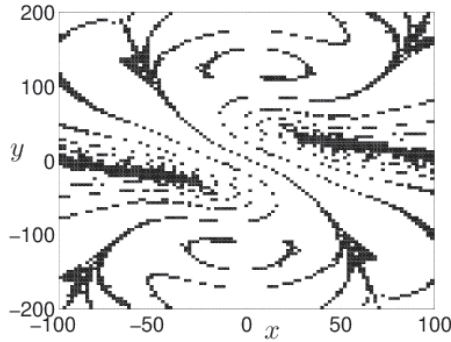


Figure 4: Regions of high finite-time Lyapunov exponent (in black) are characterized by a high sensitivity to initial conditions (i.e. high phase sensitivity). For the Lorenz model (4) (in the cross-section  $z = 319$ ), one verifies that these regions lie in the neighborhood of the fractal phaseless set (see Figure 2(c)). [The largest finite-time Lyapunov exponent is computed by using its definition [16, 30], with a finite horizon  $t = 10$ . The black region corresponds to a value higher than 0.25.]

with  $a = 0.03$  and  $\gamma = 0.06123456756432$  (which approximates an irrational number). The map has a periodic dense orbit near  $x = 0.25$  and the corresponding asymptotic phase function is characterized by a complex geometry (see Figure 5(a) or Figure 12(a) in [20])



with self-similar patterns (Figure 5(b)). In contrast to the continuous-time Lorenz system, these patterns are not observed at very small scales, but have a minimal size  $\Delta^*$  that depends on the distance to the limit cycle (Figure 6). (Note that the patterns have an arbitrarily small size as they are observed far from the limit cycle, i.e. for  $x \rightarrow \infty$ .) The fractal region is therefore an *almost phaseless set*  $\tilde{\mathcal{S}}$  (see [21]) rather than a phaseless set. It is characterized by a high sensitivity to initial conditions, as shown by the values of the largest finite-time Lyapunov exponent (Figure 7). In contrast to the case of continuous-time systems, the almost phaseless set cannot be interpreted in terms of a fractal chaotic saddle, i.e. all trajectories—including those with the initial conditions in  $\tilde{\mathcal{S}}$ —converge to the limit cycle.

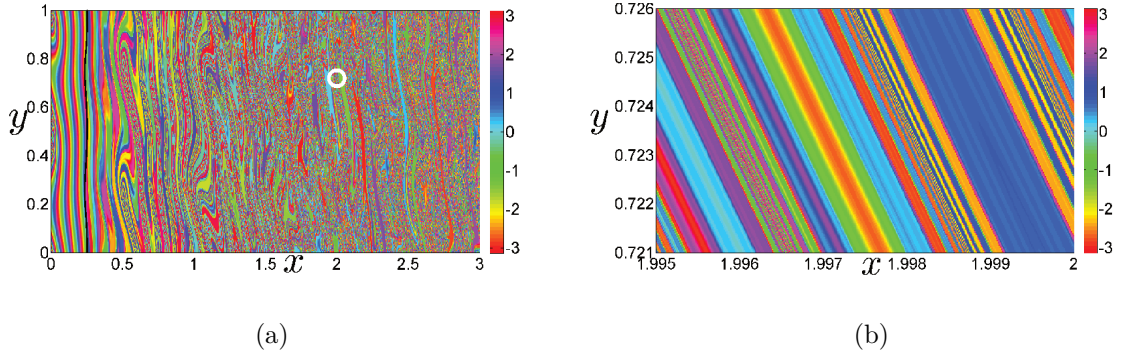


Figure 5: (a) The asymptotic phase associated with the discrete map (5) is characterized by complex patterns. The black curve is the invariant dense orbit. (b) A close-up in a region of the state space (marked with the white circle in (a)) shows the almost fractal property of the asymptotic phase.

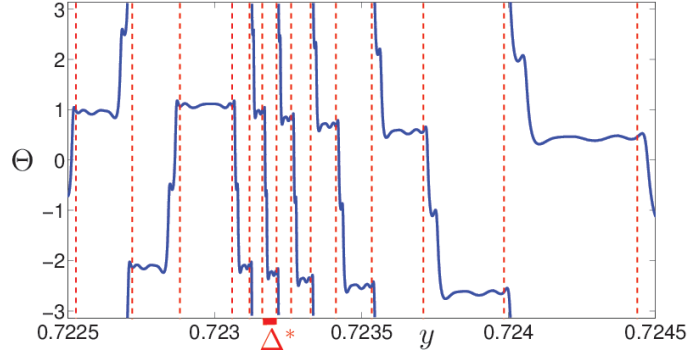


Figure 6: For the map (5), the phase function along the line  $x = 2$  shows that self-similar patterns (separated by the red dashed lines) are not observed at every scale. The size  $\Delta^*$  of the smallest pattern is of the order of  $3 \times 10^{-5}$ . (The resolution of the curve is  $6.67 \times 10^{-8}$ .)

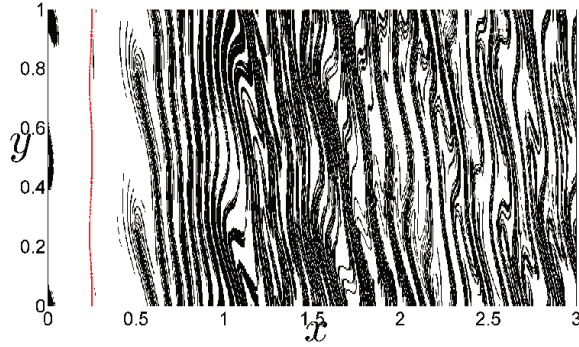


Figure 7: For the map (5), regions of high finite-time Lyapunov exponent (in black) are characterized by a high sensitivity to initial conditions (i.e. high phase sensitivity). These regions lie in the neighborhood of the fractal almost phaseless set. The red curve is the invariant dense orbit. [The largest finite-time Lyapunov exponent is computed over 35 iterations of the map. The black region corresponds to a value higher than 0.1.]

#### IV. PHASE SENSITIVITY AND FRACTAL DIMENSION

Phaseless sets are always characterized by a high sensitivity of the asymptotic phase. But when they have a fractal geometry, they occupy an important portion of the state space, so that the overall phase sensitivity of the system is accentuated. The largest Lyapunov exponent cannot capture this overall phase sensitivity, since it is always equal to zero (the

finite-time Lyapunov exponent tends to zero as the time horizon increases). Therefore, a new notion is required to measure the overall phase sensitivity of the system. To this end, we define a *phase sensitivity coefficient* and we show that this coefficient is closely related to the fractal dimension of the isochrons.

### A. Phase sensitivity

Consider the geodesic distance  $d : \mathbb{S}^1 \times \mathbb{S}^1 \rightarrow [0, \pi)$  on the circle

$$d(\theta, \theta') = \min_{k \in \mathbb{Z}} |\theta - \theta' + k2\pi|. \quad (6)$$

We define the *phase sensitivity function*  $f : \mathcal{B} \times \mathbb{R}^+ \rightarrow [0, \pi)$  by

$$f(\mathbf{x}, \epsilon) = \max_{\mathbf{x}' \in B(\mathbf{x}, \epsilon) \cap \mathcal{B}} d(\Theta(\mathbf{x}), \Theta(\mathbf{x}')),$$

where  $B(\mathbf{x}, \epsilon)$  is a ball with center  $\mathbf{x}$  and radius  $\epsilon > 0$ . If there is an uncertainty  $\epsilon$  (e.g. induced by external perturbations or noise) on the initial condition  $\mathbf{x}$  of a trajectory, then the asymptotic behavior of the trajectory will be associated with an uncertainty  $f(\mathbf{x}, \epsilon)$  on the phase. Note that  $f(\mathbf{x}, \epsilon)$  is the worst-case uncertainty.

For a given compact subset  $\mathcal{A} \subset \mathbb{R}^n$  of the state space, the average phase sensitivity function is computed as

$$\langle f(\mathbf{x}, \epsilon) \rangle_{\mathcal{A} \cap \mathcal{B}} = \frac{1}{\mu[\mathcal{A} \cap \mathcal{B}]} \int_{\mathcal{A} \cap \mathcal{B}} f(\mathbf{x}, \epsilon) d\mathbf{x},$$

where  $\mu$  is the Lebesgue measure on  $\mathcal{A}$ . Finally we define

$$\alpha = \lim_{\epsilon \rightarrow 0} \frac{\ln \langle f(\mathbf{x}, \epsilon) \rangle_{\mathcal{A} \cap \mathcal{B}}}{\ln \epsilon} \quad \beta = 1 - \lim_{\epsilon \rightarrow 0} \frac{\ln \langle f(\mathbf{x}, \epsilon) \rangle_{\mathcal{A} \cap \mathcal{B}}}{\ln \epsilon}, \quad (7)$$

or equivalently,  $\langle f(\mathbf{x}, \epsilon) \rangle_{\mathcal{A} \cap \mathcal{B}} \sim \epsilon^\alpha = \epsilon^{1-\beta}$  for  $\epsilon \ll 1$ . We refer to  $\beta = 1 - \alpha$  as the *phase sensitivity coefficient*. If  $\beta = 0$ , reducing the uncertainty  $\epsilon$  on the initial condition by a certain amount (e.g. reducing the noise intensity) reduces the average phase uncertainty by the same amount (at least when  $\epsilon$  is small). This is the usual situation observed with globally asymptotically stable periodic systems (e.g. Van der Pol model, see Figure 1). But if the phase function has fractal properties, we observe that  $\beta > 0$ . In this case, a reduction of the uncertainty  $\epsilon$  produces only a slight reduction of the average phase uncertainty. For instance, in the Lorenz model considered in Section III A, we compute a phase sensitivity

coefficient  $\beta \approx 0.65$  (see Figure 8). In this case, a reduction of the uncertainty  $\epsilon$  by a factor 2 only reduces the average phase uncertainty by a factor  $2^{1-0.65} \approx 1.27$ . The phase sensitivity coefficient is therefore directly related to the overall phase sensitivity of the system.

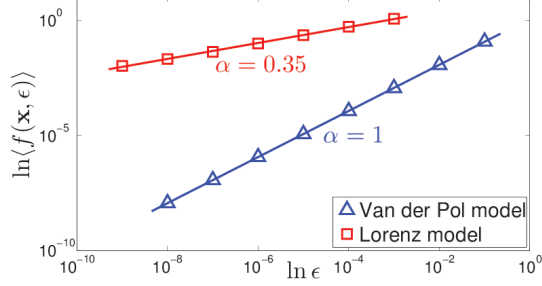


Figure 8: When the phase function exhibits fractal patterns, the phase sensitivity coefficient  $\beta = 1 - \alpha$  is greater than 0. We obtain  $\beta = 0$  for the Van der Pol model (see Figure 1), and  $\beta = 0.65$  for the Lorenz model (4). [For the Van der Pol model, we have considered the (one-dimensional) set  $\mathcal{A} = [-3, 3] \times \{1\}$ . The phase sensitivity function  $f$  is approximated by considering only two phases on the ball  $B(\mathbf{x}, \epsilon)$ , i.e.  $f \approx \max_{\mathbf{x}' \in \{\mathbf{x}'_1, \mathbf{x}'_2\}} d(\Theta(\mathbf{x}), \Theta(\mathbf{x}'))$ , with  $\mathbf{x}'_1 = (x + \epsilon, y)$  and  $\mathbf{x}'_2 = (x - \epsilon, y)$ . The average  $\langle f \rangle$  is computed over 1000 points equally distributed in  $\mathcal{A}$ . For the Lorenz model, we have considered the set  $\mathcal{A} = [-48.8, -48.75] \times \{100\} \times \{319\}$  (in the close-up of Figure 2(d)). The phase sensitivity function is approximated with two points  $(x + \epsilon, y, z)$  and  $(x - \epsilon, y, z)$  and its average is computed over 2500 points equally distributed in  $\mathcal{A}$ .]

## B. Fractal dimension

We now show that the phase sensitivity coefficient (7) is closely related to the fractal co-dimension of the phaseless set and the isochrons. For a given  $\epsilon > 0$ , consider the set

$$\mathcal{M}_{\mathcal{S}}(\epsilon) = \{\mathbf{x} \in \mathcal{A} \cap \mathcal{B} | B(\mathbf{x}, \epsilon) \cap \mathcal{S} \neq \emptyset\},$$

i.e. the sets of points lying within a distance  $\epsilon$  of the phaseless set  $\mathcal{S}$ . If there is no phaseless set in  $\mathcal{A}$ , we consider by convention that  $\mathcal{M}_{\mathcal{S}}(\epsilon) = \emptyset$ . Since the values of the phase function span  $\mathbb{S}^1$  on any neighborhood of  $\mathcal{S}$ , we have

$$f(\mathbf{x}, \epsilon) = \pi \quad \forall \mathbf{x} \in \mathcal{M}_{\mathcal{S}}(\epsilon). \quad (8)$$

If the limit cycle  $\Gamma$  is normally hyperbolic, the isochrons are as smooth as the vector field, and so is the phase function  $\Theta$  in  $\mathcal{B}$ , since  $\Theta$  smoothly increases from one isochron to another. It follows that, for  $\epsilon$  small enough and  $\delta\epsilon > 0$ , we have

$$f(\mathbf{x}, \epsilon) = \max_{\|\mathbf{e}\|=\epsilon} |\nabla\Theta(\mathbf{x}) \cdot \mathbf{e}| + \mathcal{O}(\epsilon^2) = \epsilon \|\nabla\Theta(\mathbf{x})\| + \mathcal{O}(\epsilon^2) \quad \forall \mathbf{x} \in \mathcal{A} \cap \mathcal{B} \setminus \mathcal{M}_{\mathcal{S}}(\epsilon + \delta\epsilon), \quad (9)$$

where  $\nabla\Theta$  is the gradient of the phase function. Then (8) and (9) imply that

$$\begin{aligned} \langle f(\mathbf{x}, \epsilon) \rangle_{\mathcal{A} \cap \mathcal{B}} &= \frac{1}{\mu[\mathcal{A} \cap \mathcal{B}]} \left( \int_{\mathcal{M}_{\mathcal{S}}(\epsilon)} f(\mathbf{x}, \epsilon) d\mathbf{x} + \int_{\mathcal{A} \cap \mathcal{B} \setminus \mathcal{M}_{\mathcal{S}}(\epsilon + \delta\epsilon)} f(\mathbf{x}, \epsilon) d\mathbf{x} + \int_{\mathcal{M}_{\mathcal{S}}(\epsilon + \delta\epsilon) \setminus \mathcal{M}_{\mathcal{S}}(\epsilon)} f(\mathbf{x}, \epsilon) d\mathbf{x} \right) \\ &= \frac{\mu[\mathcal{M}_{\mathcal{S}}(\epsilon)]}{\mu[\mathcal{A} \cap \mathcal{B}]} \pi + \left( 1 - \frac{\mu[\mathcal{M}_{\mathcal{S}}(\epsilon + \delta\epsilon)]}{\mu[\mathcal{A} \cap \mathcal{B}]} \right) \epsilon \langle \|\nabla\Theta\| \rangle_{\mathcal{A} \cap \mathcal{B} \setminus \mathcal{M}_{\mathcal{S}}(\epsilon + \delta\epsilon)} \\ &\quad + \frac{1}{\mu[\mathcal{A} \cap \mathcal{B}]} \int_{\mathcal{M}_{\mathcal{S}}(\epsilon + \delta\epsilon) \setminus \mathcal{M}_{\mathcal{S}}(\epsilon)} f(\mathbf{x}, \epsilon) d\mathbf{x} + \mathcal{O}(\epsilon^2). \end{aligned}$$

Since by definition  $0 \leq f(x, \epsilon) \leq \pi$ , one has

$$0 \leq \int_{\mathcal{M}_{\mathcal{S}}(\epsilon + \delta\epsilon) \setminus \mathcal{M}_{\mathcal{S}}(\epsilon)} f(\mathbf{x}, \epsilon) d\mathbf{x} \leq \mu[\mathcal{M}_{\mathcal{S}}(\epsilon + \delta\epsilon) \setminus \mathcal{M}_{\mathcal{S}}(\epsilon)] \pi$$

and it follows that

$$\begin{aligned} &\frac{\mu[\mathcal{M}_{\mathcal{S}}(\epsilon)]}{\mu[\mathcal{A} \cap \mathcal{B}]} \pi + \left( 1 - \frac{\mu[\mathcal{M}_{\mathcal{S}}(\epsilon + \delta\epsilon)]}{\mu[\mathcal{A} \cap \mathcal{B}]} \right) \epsilon \langle \|\nabla\Theta\| \rangle_{\mathcal{A} \cap \mathcal{B} \setminus \mathcal{M}_{\mathcal{S}}(\epsilon + \delta\epsilon)} + \mathcal{O}(\epsilon^2) \\ &\leq \langle f(\mathbf{x}, \epsilon) \rangle_{\mathcal{A} \cap \mathcal{B}} \leq \frac{\mu[\mathcal{M}_{\mathcal{S}}(\epsilon + \delta\epsilon)]}{\mu[\mathcal{A} \cap \mathcal{B}]} \pi + \left( 1 - \frac{\mu[\mathcal{M}_{\mathcal{S}}(\epsilon + \delta\epsilon)]}{\mu[\mathcal{A} \cap \mathcal{B}]} \right) \epsilon \langle \|\nabla\Theta\| \rangle_{\mathcal{A} \cap \mathcal{B} \setminus \mathcal{M}_{\mathcal{S}}(\epsilon + \delta\epsilon)} + \mathcal{O}(\epsilon^2). \end{aligned}$$

Considering  $\delta\epsilon = \epsilon$  and taking the limit  $\epsilon \rightarrow 0$  yield

$$\begin{aligned} &\lim_{\epsilon \rightarrow 0} \frac{\ln \left( \mu[\mathcal{M}_{\mathcal{S}}(2\epsilon)] \pi + (1 - \mu[\mathcal{M}_{\mathcal{S}}(2\epsilon)] / \mu[\mathcal{A} \cap \mathcal{B}]) \epsilon \langle \|\nabla\Theta\| \rangle_{\mathcal{A} \cap \mathcal{B} \setminus \mathcal{M}_{\mathcal{S}}(2\epsilon)} \right)}{\ln \epsilon} \\ &\leq \alpha \leq \lim_{\epsilon \rightarrow 0} \frac{\ln \left( \mu[\mathcal{M}_{\mathcal{S}}(\epsilon)] \pi + (1 - \mu[\mathcal{M}_{\mathcal{S}}(2\epsilon)] / \mu[\mathcal{A} \cap \mathcal{B}]) \epsilon \langle \|\nabla\Theta\| \rangle_{\mathcal{A} \cap \mathcal{B} \setminus \mathcal{M}_{\mathcal{S}}(2\epsilon)} \right)}{\ln \epsilon}. \end{aligned} \quad (10)$$

If  $\mathcal{M}_{\mathcal{S}}(\epsilon) = \emptyset$ , we have simply

$$\alpha = \lim_{\epsilon \rightarrow 0} \frac{\ln (\epsilon \langle \|\nabla\Theta\| \rangle_{\mathcal{A} \cap \mathcal{B}})}{\ln \epsilon} = 1 \quad \beta = 0.$$

Otherwise, according to [19],  $\mu[\mathcal{M}_{\mathcal{S}}(\epsilon)]$  scales as

$$\mu[\mathcal{M}_{\mathcal{S}}(\epsilon)] \sim \epsilon^{N-D}, \quad (11)$$

with  $N$  the dimension of the state space and  $D$  the capacity dimension [3] (or box-counting dimension) of the fractal set  $\mathcal{S}$ . In addition, if  $\mathcal{S}$  is a normally hyperbolic repeller of co-dimension (at most) one, the gradient  $\|\nabla\Theta\|$  scales as  $1/\epsilon$  when it is evaluated at a small

distance  $\epsilon$  of  $\mathcal{S}$  (see Appendix A), so that  $\langle \|\nabla\Theta\| \rangle_{\mathcal{A} \cap \mathcal{B} \setminus \mathcal{M}_{\mathcal{S}}(2\epsilon)} \sim \ln \epsilon$  for  $\epsilon \ll 1$  [32]. Finally, (10) leads to

$$\lim_{\epsilon \rightarrow 0} \frac{\ln \left( (2\epsilon)^{N-D} + (1 - (2\epsilon)^{N-D}) \epsilon \ln \epsilon \right)}{\ln \epsilon} \leq \alpha \leq \lim_{\epsilon \rightarrow 0} \frac{\ln \left( \epsilon^{N-D} + (1 - (2\epsilon)^{N-D}) \epsilon \ln \epsilon \right)}{\ln \epsilon}$$

or equivalently

$$\alpha = N - D \quad \beta = 1 - (N - D) \quad (12)$$

(for  $\mathcal{S}$  of co-dimension less or equal to one). This important relationship implies that the phase sensitivity coefficient is directly related to the fractal dimension of  $\mathcal{S}$ . More precisely, the coefficient will be strictly greater than 0 only if  $\mathcal{S}$  is fractal. Note that a phaseless set  $\mathcal{S}$  of co-dimension greater than 1 is associated with a phase sensitivity coefficient equal to 0, even if it is fractal.

When the phaseless set  $\mathcal{S}$  is fractal, the isochrons themselves are also fractal. Consider an isochron  $\mathcal{I}_\theta$ , with a capacity dimension  $D_{\mathcal{I}}$ . Since any neighborhood of  $\mathcal{S}$  intersects  $\mathcal{I}_\theta$  [6], every box of size  $\epsilon$  used to cover  $\mathcal{S}$  intersects  $\mathcal{I}_\theta$ . Hence, we have

$$N_{\mathcal{I}}(\epsilon) \geq N_{\mathcal{S}}(\epsilon),$$

where  $N_{\mathcal{S}}(\epsilon)$  and  $N_{\mathcal{I}}(\epsilon)$  are the number of boxes of size  $\epsilon$  required to cover  $\mathcal{S}$  and  $\mathcal{I}_\theta$ , respectively. It follows that, for  $\epsilon < 1$

$$\frac{N_{\mathcal{I}}(\epsilon)}{\log(1/\epsilon)} \geq \frac{N_{\mathcal{S}}(\epsilon)}{\log(1/\epsilon)}$$

and we have finally

$$D_{\mathcal{I}} = \lim_{\epsilon \rightarrow 0} \frac{N_{\mathcal{I}}(\epsilon)}{\log(1/\epsilon)} \geq \lim_{\epsilon \rightarrow 0} \frac{N_{\mathcal{S}}(\epsilon)}{\log(1/\epsilon)} = D,$$

so that the capacity dimension of  $\mathcal{I}_\theta$  is greater or equal to the capacity dimension  $D$  of  $\mathcal{S}$ .

The fractal properties of  $\mathcal{S}$  (and of the isochrons) and the phase sensitivity can also be characterized by considering the set

$$\mathcal{M}_{\delta\theta}(\epsilon) = \{\mathbf{x} \in \mathcal{A} \cap \mathcal{B} | \exists \mathbf{x}' \in B(\mathbf{x}, \epsilon) \text{ s.t. } d(\Theta(\mathbf{x}), \Theta(\mathbf{x}')) > \delta\theta\}$$

for given  $\epsilon > 0$  and  $0 < \delta\theta < \pi$ . Since it is clear that  $\mathcal{M}_{\delta\theta}(\epsilon) \approx \mathcal{M}_{\mathcal{S}}(\epsilon)$  as  $\epsilon \rightarrow 0$ , (11) yields the additional relationship

$$N - D = \lim_{\epsilon \rightarrow 0} \frac{\ln \mu[\mathcal{M}_{\delta\theta}(\epsilon)]}{\ln \epsilon} \quad (13)$$

for any value  $\delta\theta$ , provided that  $\mathcal{M}_{\delta\theta}(\epsilon, \delta\theta) \neq \emptyset$ . If  $\mathcal{S}$  is fractal with  $N - D < 1$ , then the fraction of trajectories for which an uncertainty smaller than  $\epsilon$  on the initial condition induces a phase uncertainty greater than  $\delta\theta$  on the asymptotic phase will only be slightly reduced by a significant decreasing of  $\epsilon$ . We remark that this property is independent of the value  $\delta\theta$ .

The definitions and equalities (7)-(12)-(13) summarize the relationships between the overall phase sensitivity of the system and the fractal dimension of the isochrons and phaseless set. Also, the phase sensitivity coefficient provides an alternative way to compute the fractal dimension. Figure 9 compares the computation of the fractal dimension through (7)-(12) and through (13) directly. The two methods give the same results. However, the value  $\mu[\mathcal{M}_{\delta\theta}(\epsilon)]$  in (13) is usually underestimated (see Remark 1) so that the numerical computation may yield a zero value for small (but positive) values  $\epsilon$ . The computation of the phase sensitivity coefficient is therefore easier and more accurate.

**Remark 1.** For numerical computations, considering (a few) sample points on the boundary of the balls  $B(\epsilon, r)$  is valid when the phaseless set is of co-dimension 1 (or less). In that case, even though the phase sensitivity function is underestimated and the value  $\pi$  in (10) is replaced by a smaller value, the ratio (10) is still equal to  $\alpha$ . Similarly, the value  $\mu[\mathcal{M}_{\delta\theta}(\epsilon)]$  is underestimated but the ratio (13) remains unchanged.

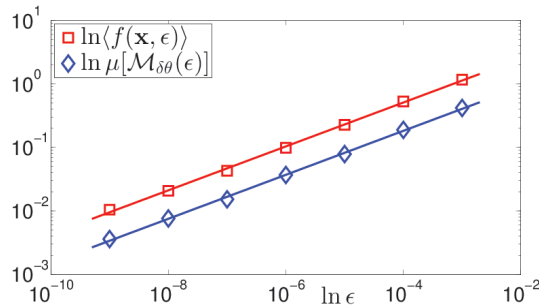


Figure 9: The fractal dimension  $D$  of the phaseless set (and of the isochrons) is computed for the Lorenz model (4), with  $\alpha$  (in red) and with the ratio (13) (in blue). The two methods yield equivalent results, both showing that the fractal dimension is equal to 2.65 ( $N - D = 0.34573$  with the first method;  $N - D = 0.34623$  with the second method). The computation details are the same as in Figure 8. For the second method, we have considered the value  $\delta\theta = 0.5$ .

*Fractal almost phaseless set.* The discrete map (5) has an almost phaseless set  $\tilde{\mathcal{S}}$  characterized by fractal patterns scaling down to  $\Delta^*$ . This implies that the phase sensitivity coefficient, as defined in (7), is equal to zero, so that the dimension  $D$  of  $\tilde{\mathcal{S}}$  is one. But for  $\epsilon > \Delta^*$ , the phase sensitivity function behaves as if the fractal dimension were more than one: the average phase sensitivity function remains close to one and slowly decreases as  $\epsilon$  decreases (see Figure 10). In other words, the “infinitesimal” phase sensitivity coefficient

$$\tilde{\beta} = 1 - \tilde{\alpha} = 1 - \frac{d \ln \langle f(\mathbf{x}, \epsilon) \rangle_{\mathcal{A} \cap \mathcal{B}}}{d \ln \epsilon}$$

is large for  $\epsilon > \Delta^*$ . In contrast, for maps that do not have an almost phaseless set with these “almost fractal” properties, the average phase sensitivity function scales as  $\epsilon^1$  for all values of  $\epsilon$  (black stars in Figure 10).

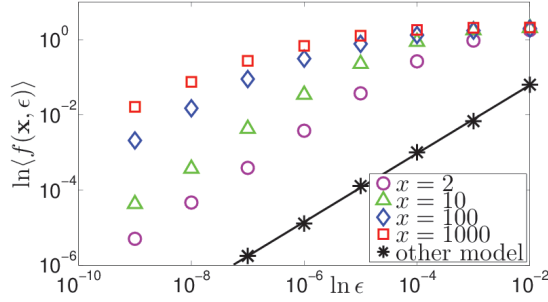


Figure 10: For the discrete time map (5), the phase sensitivity coefficient  $\beta = 1 - \alpha$  is equal to zero, as indicated by the slope  $\tilde{\alpha}$  of  $\ln \langle f \rangle$  for small values  $\epsilon$ . However, for  $\epsilon > \Delta^*$ , the average phase sensitivity function remains close to one and the slope  $\tilde{\alpha}$  is less than one, so that  $\tilde{\beta}$  is greater than zero. The phenomenon is observed on a broad interval when the set  $\mathcal{A}$  is chosen far from the limit cycle (i.e.  $x \gg 1$ ), where  $\Delta^*$  is very small. In contrast, for the model (taken from [20])  $x^+ = \gamma(x - \omega_0) + \omega_0 \bmod 1$ ,  $y^+ = y + x \bmod 1$  with  $\omega_0 = 0.5613245623$ ,  $\gamma = 0.06123456756432$ , there is no fractal (almost) phaseless set and we observe that  $\langle f \rangle \sim \epsilon$  for all values  $\epsilon$  (black stars). [The sets  $\mathcal{A}$  are one-dimensional intervals  $y \in [0, 1]$  with  $x \in \{2, 10, 100, 1000\}$  constant. The function  $f(\mathbf{x}, \epsilon)$  is approximately computed with the two points  $(x, y - \epsilon)$  and  $(x, y + \epsilon)$ . The average  $\langle f \rangle$  is computed over 10000 sample points equally distributed in  $\mathcal{A}$ .]



## V. APPLICATION TO BURSTING NEURONS

The notions of phase and isochrons play a central role in the study of neuron models, showing the sensitivity of neurons to external inputs. Motivated by preliminary observations presented in [18], we apply our results to popular (periodic) bursting neuron models (see Appendix B). We show that elliptic bursting models exhibit strong fractal properties associated with very high phase sensitivity. We briefly discuss the fractal phase response curve of those models.

### A. Phase uncertainty coefficient

Bursting is the alternation between a relatively quiescent state and a succession of rapid spikes in a system. This phenomenon is observed with slow-fast dynamics and is explained by particular bifurcations in the fast subsystems [22]. According to the types of bifurcations involved in the bursting mechanism, bursting models can be classified in different categories: elliptic bursting (subcritical Hopf bifurcation/fold limit cycle bifurcation), square-wave bursting (saddle-node bifurcation/homoclinic bifurcation), parabolic bursting (saddle-node on a limit cycle bifurcation); see [11] for more details.

As shown in Figure 11, each type of bursting is associated with a particular range of values for the phase sensitivity coefficient, an observation which reflects different values of fractal dimension and overall phase sensitivity. Elliptic bursting models (in blue) are characterized by a high phase sensitivity coefficient  $\beta = 1 - \alpha$ , and therefore by strong fractal properties. This is in agreement with the preliminary observations of [18]. In contrast, parabolic bursting models (in red) have a phase sensitivity coefficient equal to 0, thereby exhibiting no fractal properties. Square-wave bursting models (in green) correspond to the intermediate situation, with a low phase sensitivity coefficient and (almost) no fractal properties.

Our analysis based on the phase sensitivity coefficient shows that elliptic bursting models are characterized by a very high overall phase sensitivity. In this case, a small uncertainty on the input signal (or a small noise perturbation) may induce high variation in phase, and a reduction of this uncertainty only slightly reduces the uncertainty on the phase. Elliptic bursting neurons are therefore characterized by sensitive and unreliable responses to inputs. Note that the sensitivity observed here only results from the properties of the

neuron dynamics and does not depend on the type of forcing (or the type of coupling in a network). This is in contrast to high sensitivity to initial conditions usually reported in neuron models with an external input (e.g. shear-induced chaos in the periodically kicked Morris-Lecar neuron [15]).

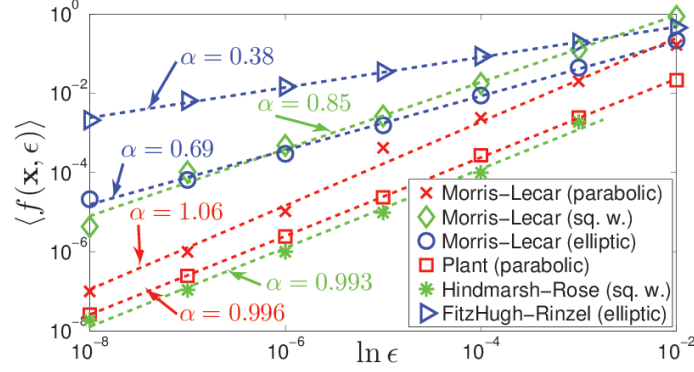


Figure 11: Elliptic bursting models (blue) are characterized by a high phase sensitivity coefficient  $\beta = 1 - \alpha$ , which corresponds to isochrons with high fractal dimension. Since they are characterized by a high overall phase sensitivity, their response to inputs is unreliable. [The sets  $\mathcal{A}$  considered in the simulations are given in Appendix B. The phase sensitivity function is approximated with two points corresponding to a perturbation  $\pm\epsilon$  along the first state component. The average of the phase sensitivity function is computed over 10000 points (2500 points for the Hindmarsh-Rose model) equally distributed in  $\mathcal{A}$ .]

## B. Fractal phase response curve

An important tool to study neuron models that admit a stable limit cycle is the well-known (finite) phase response curve

$$Z_{\mathbf{e}}(\theta) = \Theta(\mathbf{x}^\gamma(\theta) + \mathbf{e}) - \theta, \quad (14)$$

with  $\mathbf{x}^\gamma(\theta) \in \Gamma$ . It represents the phase shift of a trajectory on the limit cycle that is subjected to an instantaneous perturbation  $u(t) = \mathbf{e}\delta(t)$ , where  $\delta(t)$  is the Dirac function.

Owing to their fractal properties, elliptic bursting neuron models are characterized by a fractal phase response curve (Figure 12). The fractal dimension of this curve can be obtained

as follows. The relationship (12) implies that the isochrons—i.e. the level sets of  $\Theta$ —have a dimension  $D_{\mathcal{I}} = N - 1 + \beta$  (we assume here that  $D_{\mathcal{I}} = D$ ), so that the hypersurface  $\Lambda = \{(\mathbf{x}, \Theta(\mathbf{x})) | \mathbf{x} \in \mathcal{B}\} \subset \mathcal{B} \times \mathbb{S}^1$  is of dimension  $N + \beta$ . If we assume that the curve  $\Omega = \{\mathbf{x}^\gamma(\theta) + \mathbf{e} | \theta \in \mathbb{S}^1\}$  satisfies  $\Omega \cap \mathcal{S} \neq \emptyset$ , it follows that the curve  $\{(\mathbf{x}, \Theta(\mathbf{x})) | \mathbf{x} \in \Omega\} \subset \Lambda$  is of dimension  $N + \beta - (N - 1) = 1 + \beta$ . This implies that the dimension of the phase response curve (14) is also equal to  $1 + \beta$ .

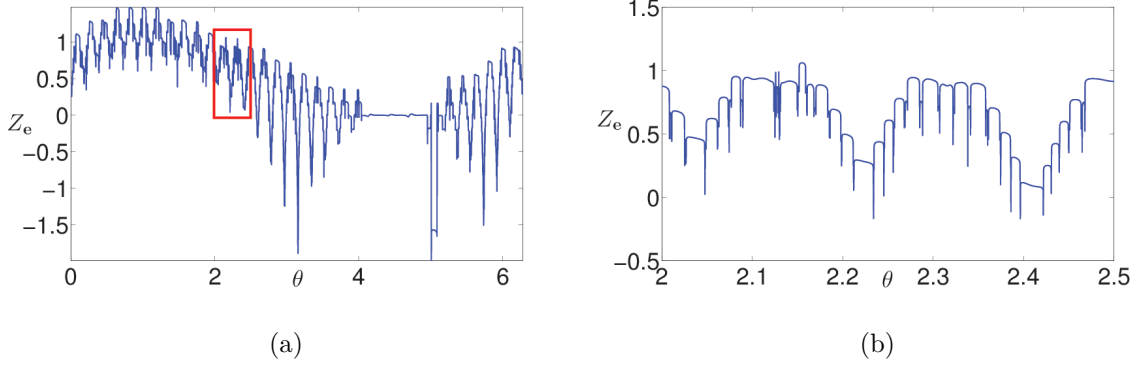


Figure 12: For the modified Morris-Lecar model in elliptic bursting regime, the phase response curve (14) is fractal, with a dimension equal to  $1 + \beta$ . Note that no fractal pattern is observed in the flat region  $\theta \in [4, 5]$ , which corresponds to the quiescent segment on the limit cycle. The perturbation  $\mathbf{e}$  is in the  $V$  direction and has a strength of 1 mV.

## VI. CONCLUSION

We have discussed the fractal properties of asymptotically periodic systems and we have provided a theoretical framework to quantify these properties. Through the notion of phase sensitivity coefficient, the fractal capacity dimension of the isochrons has been related to the overall phase sensitivity of the system.

The main implication of the results is that there exist systems—with isochrons of high fractal dimension—that are characterized by a (extremely) high phase sensitivity. For these systems, reducing the intensity of a noise perturbation only slightly decreases the average uncertainty on the phase. This is for instance the case of elliptic bursting neuron models, whose response to external inputs is unreliable.

We will finally note that the rich geometric properties of asymptotically periodic systems

illustrate the importance of developing efficient methods for computing the isochrons and the phase function. It is only when these methods are well-suited to complex dynamics in high dimensional spaces that they may unveil new properties, such as the fractal isochrons described in this paper.

### Acknowledgments

This work was funded by Army Research Office Grant W911NF-11-1-0511, with Program Manager Dr. Sam Stanton. It was completed while A. Mauroy was with the Department of Mechanical Engineering, University of California Santa Barbara.

### Appendix A: Scaling of $\|\nabla\Theta\|$

The (infinitesimal) phase difference between two trajectories

$$\Theta(\varphi^{-t}(x + dx)) - \Theta(\varphi^{-t}(x)) = \nabla\Theta(\varphi^{-t}(x))^T(\varphi^{-t}(x + dx) - \varphi^{-t}(x))$$

is constant. It follows that we have, for all infinitesimal  $dx$ ,

$$\nabla\Theta(x)^T dx = \nabla\Theta(\varphi^{-t}(x))^T M(t) dx,$$

where  $M(t)$  is the fundamental matrix solution of

$$\frac{dM}{dt} = J(\varphi^{-t}(x))M$$

and  $J$  is the Jacobian matrix of the vector field  $\mathbf{F}$ .

If we assume that  $\mathcal{S}$  is normally hyperbolic and of co-dimension (at most) 1, we can choose  $dx = dx_\perp$  in the direction tangent to the fibers of  $\mathcal{S}$  and we obtain

$$\|\nabla\Theta(x)\| \|dx_\perp\| \cos \beta(0) = \|\nabla\Theta(\varphi^{-t}(x))\| \|M(t)dx_\perp\| \cos \beta(t) \quad (\text{A1})$$

with  $\beta(t)$  the angle between the gradient  $\nabla\Theta(\varphi^{-t}(x))$  and the direction  $M(t)dx_\perp$  tangent to the fiber. Since  $\nabla\Theta(\varphi^{-t}(x)) \neq 0$  and  $M(t)dx_\perp \neq 0$  for all  $t$ , it follows that either  $\cos \beta(t) = 0$  for all  $t$  or  $\cos \beta(t) \neq 0$  for all  $t$ . The first case (i.e.  $\beta(t) = \pm\pi/2$ ) is not possible since the isochrons are not the fibers of  $\mathcal{S}$  (otherwise,  $\mathcal{S}$  would not be phaseless). For the same reason,

the isochrons are not tangent to the normal bundle of  $\mathcal{S}$  in the neighborhood of  $\mathcal{S}$ , so that one cannot have  $\cos \beta(t) \rightarrow 0$  as  $t \rightarrow \infty$ . Also, one has

$$\|M(t)dx_{\perp}\| = \mathcal{O}(e^{\lambda_{\perp}t}) \quad t \rightarrow \infty$$

where  $\lambda_{\perp}$  is the (negative) Lyapunov exponent of the system in backward time, associated with the normal direction  $dx_{\perp}$ . (Note that the value  $\exp(\lambda_{\perp})$  is the generalized Lyapunov type number along the fiber [4, 27].) It follows from (A1) that

$$\|\nabla\Theta(\varphi^{-t}(x))\| = \mathcal{O}(e^{-\lambda_{\perp}t}) \quad t \rightarrow \infty.$$

Since the distance  $d_{\mathcal{S}}$  between the trajectories and  $\mathcal{S}$  satisfies  $d_{\mathcal{S}}(\varphi^{-t}(x)) = \mathcal{O}(\exp(\lambda_{\perp}t))$  as  $t \rightarrow \infty$ , we have finally

$$\|\nabla\Theta(\varphi^{-t}(x))\| = \mathcal{O}\left(\frac{1}{d_{\mathcal{S}}(\varphi^{-t}(x))}\right).$$

## Appendix B: Bursting neuron models

### 1. Modified Morris-Lecar model (square-wave, elliptic, or parabolic bursting)

$$\begin{aligned} C \dot{V} &= -g_{Ca}m_{\infty}(V)(V - V_{Ca}) - g_K n(V - V_K) - g_L(V - V_L) \\ &\quad - g_{KC} z(h)(V - V_K) - g_{Ca} s(V - V_{Ca}) + I \\ \dot{n} &= \phi(w_{\infty}(V) - n)/\tau(V) \\ \dot{h} &= \epsilon_1(-\mu g_{Ca}m_{\infty}(V)(V - V_{Ca}) - h) \\ \dot{s} &= \epsilon_2(s_{\infty}(V) - s)/\tau_s \end{aligned}$$

with

$$\begin{aligned} m_{\infty}(V) &= 0.5 \left(1 + \tanh \frac{V - V_1}{V_2}\right) \\ w_{\infty}(V) &= 0.5 \left(1 + \tanh \frac{V - V_3}{V_4}\right) \\ s_{\infty}(V) &= 0.5 \left(1 + \tanh \frac{V - V_5}{V_6}\right) \\ z(h) &= \frac{h}{Ca_0 + h}, \\ \tau(V) &= \cosh^{-1} \frac{V - V_3}{2V_4}. \end{aligned}$$

Parameter	Square-wave	Elliptic	Parabolic
$g_{Ca}$	4	4	4
$g_K$ (mS/cm <sup>2</sup> )	8	8	8
$g_L$ (mS/cm <sup>2</sup> )	2	2	2
$V_K$ (mV)	-84	-84	-84
$V_L$ (mV)	-60	-60	-60
$V_{Ca}$ (mV)	120	120	120
$C$ (μF/cm <sup>2</sup> )	17.8	10	1
$I$ (μA/cm <sup>2</sup> )	45	120	65
$g_{KCa}$ (mS/cm <sup>2</sup> )	0.25	0.75	1
$\phi$	0.25	0.04	1.333
$\epsilon_1$	0.005	0.002	0.02
$\mu$	0.2	0.3	0.025
$\epsilon_2$	0	0	0.02
$\tau_s$ (ms)	-	-	0.05
$g_{Cas}$ (mS/cm <sup>2</sup> )	-	-	1
$Ca_0$	10	18	1
$V_1$ (mV)	-1.2	-1.2	-1.2
$V_2$ (mV)	18	18	18
$V_3$ (mV)	12	2	12
$V_4$ (mV)	17.4	30	17.4
$V_5$ (mV)	-	-	12
$V_6$ (mV)	-	-	24

Table I: Parameters of the modified Morris-Lecar model

The parameters are given in Table I. In Figure 11, the simulations were performed with the sets  $\mathcal{A} = \{-15\} \times [0.1, 0.2] \times \{12\}$  (square-wave),  $\mathcal{A} = \{30\} \times [0, 0.5] \times \{16\}$  (elliptic), and  $\mathcal{A} = \{5\} \times [0, 0.5] \times \{1.5\} \times \{0.15\}$  (parabolic).

## 2. Hindmarsh-Rose model (square-wave bursting)

$$\begin{aligned}\dot{V} &= n - aV^3 + bV^2 - h + I \\ \dot{n} &= c - dV^2 - n \\ \dot{h} &= r(\sigma(V - V_0) - h)\end{aligned}$$

The parameters are  $a = 1$ ,  $b = 3$ ,  $c = 1$ ,  $d = 5$ ,  $r = 0.001$ ,  $\sigma = 4$ ,  $V_0 = -1.6$ ,  $I = 2$ . In Figure 11, the simulation was performed with the set  $\mathcal{A} = \{0.5\} \times [-10, 4] \times \{1.9\}$ .

## 3. FitzHugh-Rinzel model (elliptic bursting)

$$\begin{aligned}\dot{V} &= V - V^3/3 - w + y + I \\ \dot{w} &= \delta(a + V - bw) \\ \dot{y} &= \mu(c - V - dy)\end{aligned}$$

The parameters are  $I = 0.3125$ ,  $a = 0.7$ ,  $b = 0.8$ ,  $c = -0.9$ ,  $d = 1$ ,  $\delta = 0.08$ , and  $\mu = 0.0001$ . In Figure 11, the simulation was performed with the set  $\mathcal{A} = \{-1\} \times [-0.5, 0.5] \times \{0.01\}$ .

## 4. Plant model (parabolic bursting)

$$\begin{aligned}C\dot{V} &= -g_{Na}m_\infty^3(V)h(V - V_{Na}) - g_{Ca}x(V - V_{Ca}) \\ &\quad - \left(g_K n^4 + \frac{k_{KC_a}c}{0.5 + c}\right)(V - V_K) - g_L(V - V_L) \\ \dot{n} &= (h_\infty(V) - h)/\tau_h(V) \\ \dot{h} &= (n_\infty(V) - n)/\tau_n(V) \\ \dot{x} &= (x_\infty(V) - x)/\tau_x \\ \dot{c} &= f(k_1x(V_{Ca} - V) - c)\end{aligned}$$

with

$$\begin{aligned} w_\infty(V) &= \frac{\alpha_\infty(V)}{\alpha_\infty(V) + \beta_\infty(V)} \quad \text{for } w = m, h, n \\ \tau_\infty(V) &= \frac{12.5}{\alpha_\infty(V) + \beta_\infty(V)} \quad \text{for } w = h, n \\ x_\infty(V) &= \frac{1}{\exp(-0.15(V + 50)) + 1} \end{aligned}$$

where

$$\begin{aligned} \alpha_m(V) &= 0.1 \frac{50 - V_s}{\exp((50 - V_s)/10) - 1} \\ \beta_m(V) &= 4 \exp((25 - V_s)/18) \\ \alpha_n(V) &= 0.01 \frac{55 - V_s}{\exp((55 - V_s)/10) - 1} \\ \beta_n(V) &= 0.125 \exp((45 - V_s)/80) \\ \alpha_h(V) &= 0.07 \exp((25 - V_s)/20) \\ \beta_h(V) &= \frac{1}{\exp((55 - V_s)/10) + 1} \end{aligned}$$

and  $V_S = 127/105V + 8265/105$ . The parameters are  $C = 1 \mu\text{F}/\text{cm}^2$ ,  $g_{Ca} = 0.004 \text{ mS}/\text{cm}^2$ ,  $g_{Na} = 4 \text{ mS}/\text{cm}^2$ ,  $g_K = 0.3 \text{ mS}/\text{cm}^2$ ,  $g_L = 0.004 \text{ mS}/\text{cm}^2$ ,  $f = 0.0003 \text{ ms}^{-1}$ ,  $g_{KCa} = 0.03 \text{ mS}/\text{cm}^2$ ,  $V_{Ca} = 140 \text{ mV}$ ,  $V_{Na} = 30 \text{ mV}$ ,  $V_K = -75 \text{ mV}$ ,  $V_{Ca} = -40 \text{ mV}$ , and  $k_1 = 0.0085 \text{ mV}^{-1}$ . In Figure 11, the simulation was performed with the set  $\mathcal{A} = \{-20\} \times [0, 1] \times \{0.4\} \times \{0.74\} \times \{0.6\}$ .

- 
- [1] E. BROWN, J. MOEHLIS, AND P. HOLMES, *On the phase reduction and response dynamics of neural oscillator populations*, Neural Computation, 16 (2004), pp. 673–715.
  - [2] G. B. ERMENTROUT AND D. H. TERMAN, *Mathematical Foundations of Neuroscience*, vol. 35, Springer, 2010.
  - [3] J. D. FARMER, E. OTT, AND J. A. YORKE, *The dimension of chaotic attractors*, Physica D: Nonlinear Phenomena, 7 (1983), pp. 153–180.
  - [4] N. FENICHEL, *Persistence and smoothness of invariant manifolds for flows*, Indiana Univ. Math. J, 21 (1971), pp. 193–226.
  - [5] P. GASPARD AND F. BARAS, *Chaotic scattering and diffusion in the Lorentz gas*, Physical Review E, 51 (1995), p. 5332.



- [6] J. GUCKENHEIMER, *Isochrons and phaseless sets*, Journal of Mathematical Biology, 1 (1975), pp. 259–273.
- [7] A. GUILLAMON AND G. HUGUET, *A computational and geometric approach to phase resetting curves and surfaces*, SIAM Journal on Applied Dynamical Systems, 8 (2009), pp. 1005–1042.
- [8] M. W. HIRSCH, C. C. PUGH, AND M. SHUB, *Invariant manifolds*, vol. 583 of Lecture Notes in Mathematics, Springer-Verlag, 1977.
- [9] F. C. HOPPENSTEADT AND E. M. IZHIKEVICH, *Weakly connected neural networks*, New York: Springer-Verlag, 1997.
- [10] G. HUGUET AND R. DE LA LLAVE, *Computation of limit cycles and their isochrons: fast algorithms and their convergence*, SIAM Journal on Applied Dynamical Systems, 12 (2013), pp. 1763–1802.
- [11] E. M. IZHIKEVICH, *Neural excitability, spiking and bursting*, International Journal of Bifurcation and Chaos, 10 (2000), pp. 1171–1266.
- [12] ———, *Dynamical Systems in Neuroscience: The Geometry of Excitability and Bursting*, MIT press, 2007.
- [13] Y. KURAMOTO, *Chemical Oscillations, Waves, and Turbulence*, Springer-Verlag, 1984.
- [14] P. LANGFIELD, B. KRAUSKOPF, AND H. M. OSINGA, *Solving Winfree’s puzzle: The isochrons in the FitzHugh-Nagumo model*, Chaos: An Interdisciplinary Journal of Nonlinear Science, 24 (2014), p. 013131.
- [15] K. K. LIN, K. C. WEDGWOOD, S. COOMBES, AND L.-S. YOUNG, *Limitations of perturbative techniques in the analysis of rhythms and oscillations*, Journal of mathematical biology, 66 (2013), pp. 139–161.
- [16] Z. Q. LU AND R. L. SMITH, *Estimating local Lyapunov exponents*, Fields Institute Communications, 11 (1997), pp. 135–151.
- [17] A. MAUROY AND I. MEZIĆ, *On the use of Fourier averages to compute the global isochrons of (quasi)periodic dynamics*, Chaos, 22 (2012), p. 033112.
- [18] A. MAUROY, B. RHOADS, J. MOEHLIS, AND I. MEZIĆ, *Global isochrons and phase sensitivity of bursting neurons*, SIAM Journal on Applied Dynamical Systems, 13 (2014), pp. 306–338.
- [19] S. W. McDONALD, C. GREBOGI, E. OTT, AND J. A. YORKE, *Fractal basin boundaries*, Physica D: Nonlinear Phenomena, 17 (1985), pp. 125–153.
- [20] I. MEZIĆ AND A. BANASZUK, *Comparison of systems with complex behavior*, Physica D:

- Nonlinear Phenomena, 197 (2004), pp. 101–133.
- [21] H. M. OSINGA AND J. MOEHLIS, *Continuation-based computation of global isochrons*, SIAM Journal on Applied Dynamical Systems, 9 (2010), pp. 1201–1228.
  - [22] J. RINZEL AND Y. S. LEE, *Dissection of a model for neuronal parabolic bursting*, Journal of Mathematical Biology, 25 (1987), pp. 653–675.
  - [23] P. SACRÉ AND R. SEPULCHRE, *Sensitivity analysis of oscillator models in the space of phase response curves: Oscillators as open systems*, IEEE Control Systems Magazine, 34 (2014), pp. 50–74.
  - [24] W. E. SHERWOOD AND J. GUCKENHEIMER, *Dissecting the phase response of a model bursting neuron*, SIAM Journal on Applied Dynamical Systems, 9 (2010), pp. 659–703.
  - [25] S. R. TAYLOR, R. GUNAWAN, L. R. PETZOLD, AND F. J. DOYLE, *Sensitivity measures for oscillating systems: Application to mammalian circadian gene network*, IEEE Transactions on Automatic Control, 53 (2008), pp. 177–188.
  - [26] T. TÉL AND M. GRUIZ, *Chaotic dynamics: an introduction based on classical mechanics*, Cambridge University Press, 2006.
  - [27] S. WIGGINS, *Normally hyperbolic invariant manifolds in dynamical systems*, vol. 105, Springer, 1994.
  - [28] A. WINFREE, *The Geometry of Biological Time*, New York: Springer-Verlag, 2001 (Second Edition).
  - [29] A. T. WINFREE, *Patterns of phase compromise in biological cycles*, Journal of Mathematical Biology, 1 (1974), pp. 73–95.
  - [30] R. C. WOLFF, *Local Lyapunov exponents: looking closely at chaos*, Journal of the Royal Statistical Society. Series B (Methodological), (1992), pp. 353–371.
  - [31] J. A. YORKE AND E. D. YORKE, *Metastable chaos: the transition to sustained chaotic behavior in the Lorenz model*, Journal of Statistical Physics, 21 (1979), pp. 263–277.
  - [32] If  $\mathcal{S}$  is of co-dimension greater than one, intuitive arguments suggest that  $\langle \|\nabla\Theta\| \rangle_{\mathcal{A}\cap\mathcal{B}\setminus\mathcal{M}_{\mathcal{S}}(2\epsilon)} = \mathcal{O}(1)$ . However, a rigorous result is beyond the scope of this paper.